Identification of Higher-Order Electronic Coherences in Semiconductors by their Signature in Four-Wave-Mixing Signals

G. Bartels and A. Stahl
Institut für Halbleitertechnik II, Rheinisch-Westfälische Technische Hochschule Aachen, Sommerfeldstraße 24, D-52056 Aachen, Germany

V. M. Axt
Institut für Theoretische Physik, Westfälische Willhelms Universität Münster, Willhelm-Klemm-Strasse 10, D-48149 Münster, Germany

B. Haase, U. Neukirch,* and J. Gutowski
Institut für Festkörperphysik, Universität Bremen, P.O. Box 330 440, D-28334 Bremen, Germany
(Received 13 July 1998)

Four-wave-mixing signals from excitons under linear-circular polarized excitation exhibit an elliptical polarization, depending on both the pulse delay and the spectral position. Besides the resonances corresponding to excitons and exciton-biexciton transitions, a breakup of the exciton line is found reflecting the influence of correlations on the four-point level. An analysis accounting for the exciton density, the bound biexciton, and the exciton-exciton scattering continuum reveals that these features are not due to an antibound two-exciton state. Instead, they result from an interference of the correlated exciton continuum with the exciton density. In addition, the modeling shows that the signals ellipticity is highly sensitive to the influences of different correlations and, therefore, allows for a discrimination of their contributions. [S0031-9007(98)08064-8]

PACS numbers: 71.35.Gg, 42.50.Md, 42.65.–k

Quantum kinetic effects have a key role in revealing the quantum nature of the matter light interaction. Therefore, the search for distinct experimental fingerprints of correlated quantum kinetics beyond the scope of the Boltzmann equation or time-dependent Hartree-Fock theory has attracted much attention in recent years [1–7]. So far, firm evidence for phonon quantum kinetics has been found by demonstrating the occurrence and the controllability [2] of phonon sidebands and by a demonstration of the limits imposed by the energy-time uncertainty [4,5]. Also for the case of Coulomb quantum kinetics in the high excitation regime specific predictions have been made [7], namely, that time-resolved four-wave-mixing (FWM) spectra should show a sideband having a frequency which scales with the plasma frequency. However, this prediction has not been experimentally verified up to now.

The dynamics of biexcitonic contributions to FWM on the other hand is a prominent example related to Coulomb quantum kinetics at moderate excitation densities [8–14]. Recently, the dependence of the exciton-exciton correlation in the scattering state continuum on a magnetic field has been investigated [11]. In this Letter we demonstrate that even for moderate excitation the correlated Coulomb quantum kinetics leads to significant effects the description of which requires one to go beyond the coherent limit. In particular, the combined dynamics of the correlated two-pair scattering continuum and exciton densities, the latter having lost their interband coherence, leads to characteristic spectral signatures of the polarization state of FWM signals. The almost perfect agreement between calculated and experimental data obtained from ZnSe quantum wells allows one to draw a conclusive picture of the processes relevant for the signal generation.

Spectrally resolved degenerate FWM experiments are performed on a 7.5 nm thin $ZnSe/ZnS_{0.06}Se_{0.94}$ single-quantum-well sample grown by molecular-beam epitaxy lattice matched to subsequently removed GaAs substrates. The exciton binding energy amounts to 20 meV. Pulses from a frequency-doubled Ti:sapphire laser are used for excitation. The incident beams with wave vectors $\mathbf{k}_1$ and $\mathbf{k}_2$ are adjusted to the same intensity. The time delay τ of the excitation pulses is defined to be positive if pulse #1 with wave vector $\mathbf{k}_1$ precedes pulse #2 with $\mathbf{k}_2$. The polarization of the exciting fields is independently chosen to be circular (σ^+ or σ^-) or linear (x: electrical field oscillating in the scattering plane; y: perpendicular to x) by use of longitudinal high-voltage KD^*P Pockels cells. The extinction ratios exceed 5000:1. Zero time delay is precisely determined by up-converting respective straylight from the two beams with the residual infrared beam of the Ti:sapphire laser. The chirp caused by the Pockels cells, polarizer cubes, and lenses has been carefully compensated for by means of a prism sequence. As a result nearly transform-limited pulses of 115 fs duration are obtained at the sample position. The self-diffracted beam in direction $2\mathbf{k}_2 - \mathbf{k}_1$ is sent through a sequence consisting of two Pockels cells and a polarizer, allowing one to determine its polarization state. The FWM signal is

 0031-9007/98/81(26)/5880(4)$15.00

subsequently spectrally resolved and detected by means of a grating spectrometer and a nitrogen-cooled CCD camera. The sample is kept at 2 K in a helium bath cryostat.

Figure 1(a) shows FWM spectra obtained in the $2\mathbf{k}_2 - \mathbf{k}_1$ direction for a delay time of $\tau = 0.25$ ps for three different polarization configurations. The results were obtained for colinear polarization ($\| \equiv yy$, dashed line), cross-linear polarization ($\perp \equiv yx$, dotted line), and a configuration with pulse #1 being σ^+ polarized and pulse #2 being x polarized (σ^+x, solid line). In all cases only the y component of the signal was detected. Note that in the case of $\|$ and $\perp$ excitation this is already the total response. In contrast, the σ^+x signal is dynamically elliptically polarized; i.e., the ellipticity and the sense of rotation depend on the frequency as well as on the delay time. Therefore, the σ^+x excitation is most sensitive to the influences of different contributions to the microscopic dynamics. The $\perp$ spectrum shows two resonances corresponding to the bound biexciton and the heavy-hole (hh) exciton, respectively, while the $\|$ spectrum is dominated by the hh-exciton line. In the σ^+x case a breakup of the hh-exciton resonance is observed. Similar structures have been found previously and attributed to an antibound two-exciton state [15–17]. The analysis described below reveals that in our case this phenomenologically based explanation does not apply. In order to allow for a more conclusive distinction we have additionally performed a detailed analysis of the polarization state. From measurements of different polarization components (σ^+, σ^-, x, y, and linearly polarized at $\pm 45°$ with respect to x) the FWM signal is fully determined except for an overall phase factor. The polarization state $\hat{\mathbf{P}} = \hat{\mathbf{P}}(\hbar\omega, \tau)$ displayed below is connected to the complex FWM polarization $\mathbf{P} = \mathbf{P}(\hbar\omega, \tau)$ by

$$\hat{\mathbf{P}}_{2\mathbf{k}_2-\mathbf{k}_1} = \exp(-i\phi)\mathbf{P}_{2\mathbf{k}_2-\mathbf{k}_1}, \tag{1}$$

$$\phi = \arctan\left[\frac{\mathrm{Im}[P_{(2\mathbf{k}_2-\mathbf{k}_1),\mathbf{x}}]}{\mathrm{Re}[P_{(2\mathbf{k}_2-\mathbf{k}_1),\mathbf{x}}]}\right], \tag{2}$$

where $\phi = \phi(\hbar\omega, \tau)$ is defined such that the x component of $\hat{\mathbf{P}}$ is real and positive. Figure 1(b) shows the experimentally determined imaginary part of the y component of $\hat{\mathbf{P}}$ as a function of the delay time τ and the energy of the emitted light. The sign of this signal determines the sense of rotation of the elliptical polarization. Here, dark areas correspond to a positive sign and light areas to a negative sign. The most remarkable feature of the data is the change of sign in the vicinity of the hh-exciton resonance. In addition, the energetic position of the peaks changes for varying delay times. At negative delays the resonance is centered at the hh position while, for later times, it is shifted first to the lower- and then to the higher-energy side. The feature due to the biexciton exhibits no such conspicuous shifts or sign changes.

In order to understand this characteristic signature we performed calculations taking into account higher-order correlations. Our approach is based on the concept of a dynamically controlled truncation of the hierarchy of higher-order density matrices [13,14]. The relevant variable for optical experiments is the single-pair transition density y_α, because it is directly related to the interband polarization. The pertinent equation for y_α in the exciton basis reads

$$\{-i\hbar(\partial_t + \gamma_y) + \hbar\omega_\alpha\}y_\alpha = \sum_p \mathcal{M}_\alpha^p E_{\mathrm{opt}}^p + \underbrace{\mathcal{Q}_y + \mathcal{Q}_{\bar{b}} + \mathcal{Q}_{\bar{n}}}_{\equiv\, \mathcal{Q}_{\mathrm{nonlinear}}}, \tag{3}$$

where $\hbar\omega_\alpha$ is the interband transition energy of exciton α and γ_y is a phenomenological damping constant. The sources on the right-hand side are split into the linear source and contributions of third and higher order $\mathcal{Q}_{\mathrm{nonlinear}}$. The linear part comprises the dipole matrix element $\mathcal{M}_\alpha^p$ and the field of the laser pulses E_{opt}^p while

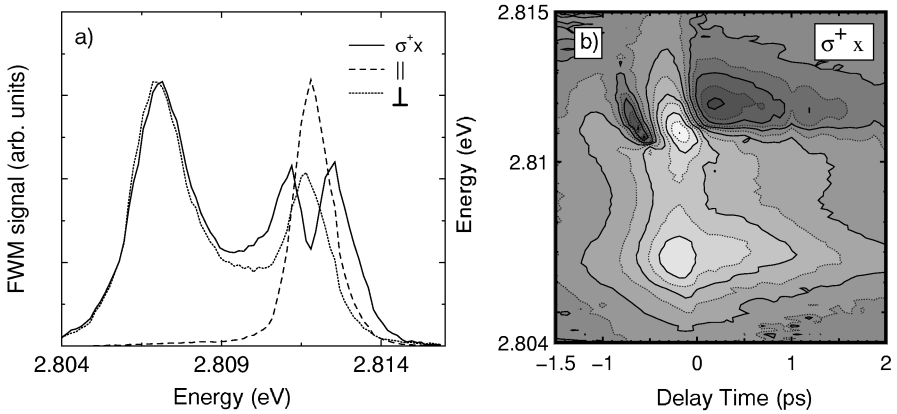

FIG. 1. (a) Experimental FWM spectra for $\tau = 0.25$ ps, normalized to the same height. The excitation polarizations were $\|$, $\perp$, and σ^+x; only the y .component of the polarization was detected; (b) contour plot of $\mathrm{Im}\{\hat{\mathbf{P}}_y\}$ as defined in Eq. (1) for σ^+x excitation. The estimated carrier density amounts to 1×10^9 cm^{-2}, corresponding to about $1/100$ of the Mott density.

the nonlinear sources are given by

$$\mathcal{Q}_y = -\sum_{p\,\bar{\alpha}\bar{\alpha}'} \mathcal{B}_{\alpha\,\bar{\alpha}}^{\bar{\alpha}'p} y_{\bar{\alpha}}^{\star} y_{\bar{\alpha}'} E_{\mathrm{opt}}^{p} + \sum_{\bar{\alpha}\bar{\alpha}'\bar{\alpha}''} (\mathcal{V}_{H_{\alpha\,\bar{\alpha}}^{\bar{\alpha}'\bar{\alpha}''}} - \mathcal{V}_{F_{\alpha\,\bar{\alpha}}^{\bar{\alpha}'\bar{\alpha}''}}) y_{\bar{\alpha}}^{\star} y_{\bar{\alpha}'} y_{\bar{\alpha}''}, \quad (4)$$

$$\mathcal{Q}_{\bar{b}} = \int_{-\infty}^{t} dt' \sum_{\alpha'\bar{\alpha}\bar{\alpha}'} y_{\bar{\alpha}}(t)^{\star} K_{\alpha\,\bar{\alpha}}^{\alpha'\bar{\alpha}'}(t - t') y_{\alpha'}(t') y_{\bar{\alpha}'}(t'), \quad (5)$$

$$\mathcal{Q}_{\bar{n}} = -\sum_{p\,\bar{\alpha}\bar{\alpha}'} \mathcal{B}_{\alpha\,\bar{\alpha}}^{\bar{\alpha}'p} \bar{n}_{\bar{\alpha}\bar{\alpha}'} E_{\mathrm{opt}}^{p} + \sum_{\bar{\alpha}\bar{\alpha}'\bar{\alpha}''} (\mathcal{V}_{H_{\alpha\,\bar{\alpha}}^{\bar{\alpha}'\bar{\alpha}''}} - \mathcal{V}_{F_{\alpha\,\bar{\alpha}}^{\bar{\alpha}'\bar{\alpha}''}}) (y_{\bar{\alpha}'} \bar{n}_{\bar{\alpha}\bar{\alpha}''} + y_{\bar{\alpha}''} \bar{n}_{\bar{\alpha}\bar{\alpha}'}), \quad (6)$$

where $\mathcal{B}$ is the matrix element of the blocking sources and $\mathcal{V}_H$, $\mathcal{V}_F$ are the Coulomb matrix elements of Hartree and Fock type, respectively. The term $\mathcal{Q}_y$ contains the Hartree-Fock contributions as well as the source for the Pauli blocking. $\mathcal{Q}_{\bar{b}}$ accounts for the two-pair contributions including the bound biexciton and the two-pair scattering continuum. Here we have made use of the memory kernel representation of two-exciton transitions introduced in Ref. 8. The kernel K is determined by an integral equation as described in [8]. Finally incoherent and intraband coherent exciton densities $\bar{n}$ enter the equations of motion via $\mathcal{Q}_{\bar{n}}$. Here, $\bar{n}$ is the exciton representation of the four-point density matrix $\bar{N}_{jj'}^{ii'} \equiv \langle (\hat{d}^i \hat{c}_j - \langle \hat{d}^i \hat{c}_j \rangle)^{\dagger} (\hat{d}^{i'} \hat{c}_{j'} - \langle \hat{d}^{i'} \hat{c}_{j'} \rangle) \rangle$, where $\hat{c}_i$ ($\hat{d}^j$) annihilate an electron (hole) [14]. The diagonal part $\bar{n}_{\alpha\alpha}$ represents the occupation density of exciton state α except for the interband coherent contribution $|y_\alpha|^2$. Furthermore, $\bar{n}_{\alpha\alpha}$ is identical to the mean square fluctuation of the exciton transition y_α. In our case it is built up exclusively by carrier-carrier interaction and is therefore of fourth order in the laser field.

Let us first focus on the influence of bound and unbound two-exciton contributions. We have calculated the memory kernel for a two-dimensional ZnSe-quantum-well model restricting the basis set to the states on the $1s$-exciton parabola, which is expected to be a good approximation due to the large exciton binding energy in ZnSe. As described in [8] the kernel is decomposed into components exhibiting either a Hartree- or a Fock-like dependence on the band indices. Figures 2(a) and 2(b) display the corresponding parts of the resulting memory kernel. The resonance of the bound biexciton is easily identified. To isolate the influence of the correlated scattering continuum the bound biexciton has been extracted from the memory kernel by fitting a single Lorentzian to the full kernel. The result is displayed in Figs. 2(c) and 2(d). An antibound state would have to show up as a resonance in the continuum which is obviously not present.

Figures 3(a) and 3(b) contain the numerical results for the imaginary part of the y component of the FWM

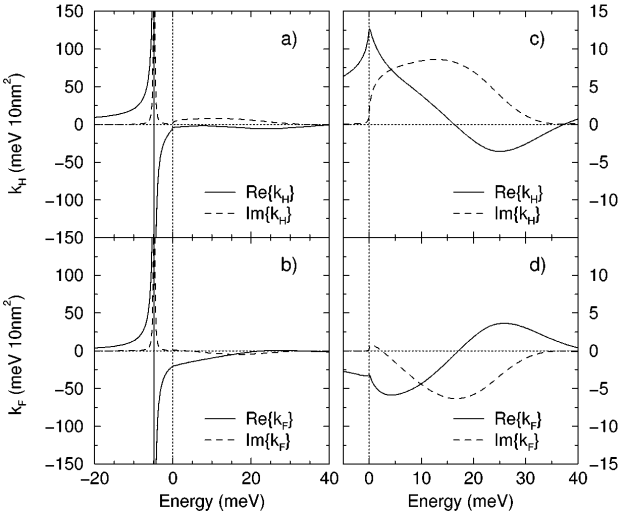

FIG. 2. The left panels show the Hartree (a) and Fock (b) part of the memory kernel obtained for a two-dimensional ZnSe-quantum-well model. The right panels show the contributions due to exciton-exciton scattering for the Hartree (c) and the Fock (d) parts of the memory kernel.

polarization introduced in Eq. (1). Part (a) has been calculated using only the bound biexciton in the memory kernel while in part (b) also the two-exciton scattering contributions have been included. Both results reproduce the experimentally found negative contribution on the spectral position of the biexciton. In contrast the signal at the hh exciton position does not show the observed behavior. Without continuum [part (a)] no negative contributions are found at all, while in the case with continuum [part (b)] the positive contributions to the signal are missing, in particular, at positive delay times. Consequently, the experimentally observed change in sign between the resonances is not reproduced on this level of the theory.

In order to include the influence of fluctuations of the exciton amplitude represented by the exciton density $\bar{n}$ the source $\mathcal{Q}_{\bar{n}}$ introduced via Eq. (6) has to be evaluated. This requires one to follow the time evolution of $\bar{n}$ determined by the equation of motion

$$\{-i\hbar(\partial_t + \gamma_{\bar{n}}) + \hbar\omega_{\alpha'} - \hbar\omega_{\alpha}\} \bar{n}_{\alpha\alpha'} = \mathcal{Q}_{\mathrm{nonlinear}}^{\star} y_{\alpha'} + y_{\alpha}^{\star} \mathcal{Q}_{\mathrm{nonlinear}}. \quad (7)$$

The FWM polarization calculated taking into account all sources in Eq. (3) including the bound biexciton, the exciton-exciton continuum, as well as the exciton densities $\bar{n}$ does not exhibit the shortcomings of the previous results. As can be seen in Fig. 3(c) we now obtain a very good agreement with the experimental result of Fig. 1(b). The distinct peaks in the vicinity of the exciton line exhibit the same complex dependence of the sign on energy and delay as found experimentally. Also the slight energetic shifts with respect to the exciton line are well reproduced by our calculation. Even the detailed shape of the contours displayed in Figs. 1(b) and 3(c) are in good agreement.

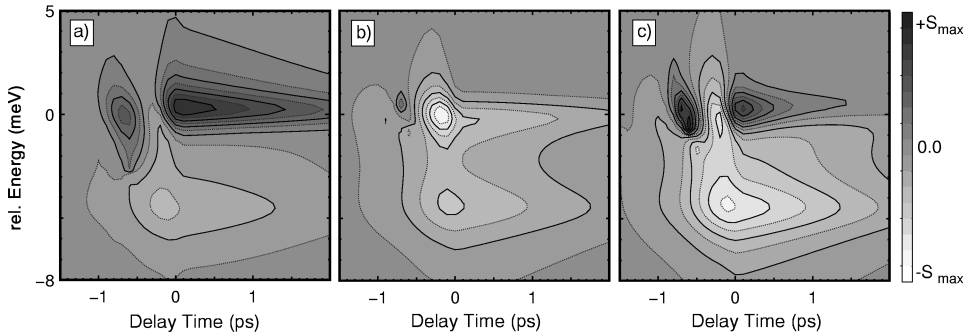

FIG. 3. Theoretical results for $\mathrm{Im}\{\hat{\mathbf{P}}_y\}$ calculated considering (a) only excitonic and biexcitonic bound states and no exciton densities; (b) the bound states and the two-exciton scattering continuum; (c) the bound states, the two-exciton continuum, and the exciton densities. An inhomogeneous broadening of the band gap of 0.7 meV has been included phenomenologically by convoluting the homogeneous result with a Gaussian. The gray levels are set linearly, with black (white) corresponding to positive (negative) signal contributions with the same absolute value $S_{\max}$ in arbitrary units.

In conclusion, this Letter demonstrates that the polarization state in FWM spectra clearly reveals the influence of three distinct electronic four-point coherences: viz. the biexciton amplitude, the exciton-exciton scattering continuum, and fluctuations of the exciton amplitude. All basic features of the complex spectral signature observed in measurements on ZnSe are satisfactorily explained within an extended density-matrix dynamics where the above mentioned four-point coherences are accounted for on a quantum-kinetic level. In particular, the additional spectral features at the exciton position are perfectly reproduced, although there is no antibound two-exciton state entering the description. These spectral structures can be naturally explained within our theory as an interference of the four-point exciton density $\bar{n}$ with the correlated part of the exciton-exciton scattering continuum.

We gratefully acknowledge inspiring discussions with T. Kuhn and H. Kurz. The authors thank M. Behringer for preparing the high-quality sample by MBE in the group of D. Hommel at Bremen University. This work has been supported by the Deutsche Forschungsgemeinschaft (DFG).

*Present address: Materials Sciences Division, MS 2-346, Lawrence Berkeley National Laboratory, 1 Cyclotron Road, Berkeley, CA 94720.

[1] J. Schilp, T. Kuhn, and G. Mahler, Phys. Rev. B **50**, 5435 (1994); Phys. Status Solidi (b) **188**, 417 (1995).

[2] M. U. Wehner, M. H. Ulm, D. S. Chemla, and M. Wegener, Phys. Rev. Lett. **80**, 1992 (1998).

[3] R. Zimmermann, J. Wauer, A. Leitenstorfer, and C. Fürst, J. Lumin. **76–77**, 34 (1998).

[4] C. Fürst, A. Leitenstorfer, A. Laubereau, and R. Zimmermann, Phys. Rev. Lett. **78**, 3733 (1997).

[5] A. Leitenstorfer, C. Fürst, A. Laubereau, and R. Zimmermann, Phys. Status Solidi B **204**, 300 (1997).

[6] U. Hohenester and W. Pötz, Phys. Rev. B **56**, 13 177 (1997).

[7] Q. T. Vu, L. Banyai, P. I. Tamborenea, and H. Haug, Europhys. Lett. **40**, 323 (1997).

[8] V. M. Axt, K. Victor, and T. Kuhn, Phys. Status Solidi (b) **206**, 189 (1998).

[9] K. Victor and A. Stahl, in *Proceedings of the 23rd International Conference on the Physics of Semiconductors, Berlin, 1996*, edited by M. Scheffler and R. Zimmermann (World Scientific, Singapore, 1996), pp. 709.

[10] T. Östreich, K. Schönhammer, and L. J. Sham, Phys. Rev. Lett. **75**, 2554 (1995).

[11] P. Kner, S. Bar-Ad, M. V. Marquezini, D. S. Chemla, and W. Schäfer, Phys. Rev. Lett. **78**, 1319 (1997).

[12] P. Kner, S. Bar-Ad, M. V. Marquezini, D. S. Chemla, and W. Schäfer, Phys. Status Solidi A **164**, 579 (1997).

[13] V. M. Axt and A. Stahl, Z. Phys. B **93**, 195 (1994); **93**, 205 (1994).

[14] V. M. Axt and S. Mukamel, Rev. Mod. Phys. **70**, 145 (1998).

[15] T. Häupl, H. Nickolaus, F. Henneberger, and A. Schülzgen, Phys. Status Solidi B **194**, 219 (1996).

[16] H. Nickolaus and F. Henneberger, Phys. Rev. B **57**, 8774 (1998).

[17] Hailong Zhou, A. V. Nurmikko, C.-C. Chu, J. Han, W.-L. Chen, and R. L. Gunshor, in *International Quantum Electronics Conference*, 1998 OSA Technical Digest Series Vol. 7 (Optical Society of America, Washington, DC, 1998), p. 212.